instruments

MDPI

Article

Acoustic Communication Among Smart Sensors: A Feasibility Study

Paolo Caruso [1,*], Helbert da Rocha [2,3], Antonio Espírito-Santo [2,3], Vincenzo Paciello [1] and José Salvado [2,3]

[1] Department of Industrial Engineering, University of Salerno, 84084 Fisciano, Italy; vpaciello@unisa.it
[2] Department of Electromechanical Engineering, University of Beira Interior, 6200-001 Covilhã, Portugal; helbert.rocha@ubi.pt (H.d.R.); aes@ubi.pt (A.E.-S.); jose.salvado@ubi.pt (J.S.)
[3] Instituto de Telecomunicações, Delegação da Covilhã, 1049-001 Lisboa, Portugal
* Correspondence: pcaruso@unisa.it

Abstract: Smart sensors and networks have spread worldwide over the past few decades. In the industry field, these concepts have found an increasing quantity of applications. The omnipresence of smart sensor networks and smart devices, especially in the industrial world, has contributed to the emergence of the concept of Industry 4.0. In a world where everything is interconnected, communication among smart devices is critical to technological development in the field of smart industry. To improve communication, many engineers and researchers implemented methods to standardize communication along the various levels of the ISO-OSI model, from hardware design to the implementation and standardization of different communication protocols. The objective of this paper is to study and implement an unconventional type of communication, exploiting acoustic wave propagation on metallic structures, starting from the state of the art, and highlighting the advantages and disadvantages found in existing literature, trying to overcome them and describing the progress beyond the state of the art. The proposed application for acoustic communication targets the field of smart industries, where implementing signal transmission via wireless or wired methods is challenging due to interference from the widespread presence of metallic structures. This study explores an innovative approach to acoustic communication, with a particular focus on the physical challenges related to acoustic wave propagation. Additionally, communication performance is examined in terms of noise rejection, analyzing the impact of injected acoustic noise on communication efficiency.

Keywords: smart sensors; smart networks; metallic structures; smart industry; acoustic communication

Citation: Caruso, P.; da Rocha, H.; Espírito-Santo, A.; Paciello, V.; Salvado, J. Acoustic Communication Among Smart Sensors: A Feasibility Study. *Instruments* **2024**, *8*, 51. https://doi.org/10.3390/instruments8040051

Academic Editor: Antonio Ereditato

Received: 27 September 2024
Revised: 11 November 2024
Accepted: 19 November 2024
Published: 22 November 2024

1. Introduction

Over the past century, research in metallurgy and the field of metal mechanics has played a vital role. In recent years, many human workers have been replaced by advanced machines capable of enhancing productivity and accelerating the pace of work and manufacturing [1]. However, the industrial world still faces difficulties implementing modern technologies such as smart sensor networks and intelligent communications [2]. The main problems in implementing smart factories and smart manufacturing in this field are communication problems among different types of machinery. As an example, in the field of metal welding, there are a lot of electrical and electromagnetic disturbances, such as sparks or radiated and conducted noise, which implement innovative technologies that are particularly challenging in such a difficult environment [3]. The main challenge is the widespread presence of metal structures in these industries, which act as electromagnetic shields and nearly block wireless communication. The shielding behavior of metal structures is explained by Equation (1), which provides the formula for the attenuation term of an electric field propagating through a material characterized by conductivity σ.

$$E(z) = E_0 e^{-\sqrt{\frac{\mu\sigma\omega}{2}}\, z} \tag{1}$$

where z is the distance traveled by the electromagnetic wave, ω is the frequency of the propagating field, and μ is the magnetic permeability of the medium through which the wave propagates. As can be seen from Equation (1), as σ increases, the wave attenuation through the material increases. For this reason, wireless communication around metal structures becomes almost impossible since metal is characterized by a high conductivity and transmission paths become highly attenuating. In addition, regarding communication through walls, some structures are characterized by steel structures present in concrete walls. This aspect is thoroughly addressed in [4], where it is demonstrated that establishing concrete communication at frequencies lower than conventional radio bands (such as 900 MHz or 2.4 GHz) is feasible.

Another potential approach is communication, using the conductivity of metal structures to send electrical signals through the metal surface. This strategy has been discussed extensively in [5]. It has many advantages, such as a low signal attenuation and, mainly, the possibility of using an existing communication infrastructure. On the other hand, this method is inefficient because it requires the presence of at least two electric conductors to establish a current loop. For this reason, it is cost-effective in terms of installation costs. However, it becomes ineffective in environments like smart welding or in communication on exposed metal structures, where multiple smart sensors need to be installed on a shared metal surface.

A suitable alternative is Visible Light Communication (VLC), as discussed in detail in [6]. VLC has many advantages regarding invasiveness and installation costs. At the same time, the productive process could disrupt the communication medium, as sparks produced by some methods, such as welding, can occasionally obfuscate the photoelectric transducers. However, it can be inconvenient because the space must be organized so that there are no obstacles between the modulated lights and the light sensors.

Despite all these problems, applications in harsh environments have been under research in recent years to implement smart technologies and communications to bring this field to the same technological level as others [7]. The objective of this paper is to introduce a groundbreaking method for enabling communication in extremely challenging industrial environments: utilizing acoustic waves transmitted through metallic structures. This approach directly addresses the key obstacles in the presented state of the art, including the unique properties and challenges of metallic media, offering an in-depth characterization of this unconventional communication channel.

Article Structure

An example of a harsh environment was provided, and the problems and challenges related to implementing communication in the smart industry, the proposed solution of acoustic waves, and the novelty introduced in this paper are discussed. Section 2 gives a background of the literature and the authors' previous works used as the foundation for the current article. Section 2.1 focuses on the contribution of the present paper to the existing literature and the different approaches to implementing communication among smart nodes in metallic structures. Section 3 presents a set of experimental setups designed to characterize typical acoustic communication through metallic structures. This section is composed of Section 3.1 (acoustic characterization of aluminum bars and noise evaluation) and Section 3.2 (implementation of improved acoustic communication). Section 4 presents the evaluation of the noise influence on the transmitted bitstrings. After these tests, the discussion and conclusion of this study will be drawn, and future directions will be presented in Section 5.

2. Background

In recent years, several researchers have explored communication via acoustic waves. Specifically, Ref. [8] offers a comprehensive study of the physical characteristics of metal structures and their behavior under vibrations induced by acoustic waves, employing Orthogonal Frequency-Division Multiplexing (OFDM) modulation. Additionally, Ref. [9]

investigates the feasibility of data transmission by modulating an acoustic signal using Multiple Frequency-Shift Keying (MFSK). Another example of acoustic communication is presented in [10], where images are transmitted along a metallic pipe using Amplitude Shift Keying (ASK) modulation to encrypt and packetize the transmitted data. These modulation techniques offer advantages such as improved symbol encoding and compatibility with fading channels. However, a key drawback is the increased computational complexity required for modulation and demodulation.

Acoustic communication has been implemented in the past with various applications. For example, the use of acoustic waves to communicate inside a nuclear facility is presented in [11]. The advantage of using this method is that nuclear facilities are often characterized by many steel structures and pipes, around which it is almost impossible to establish a wireless connection between any smart node. Furthermore, other factors like obstacles, multipath, and so on are investigated in [10], which shows how data transmission performance is affected by signal-degrading factors such as those described above. The report also discusses the slight influence of concrete walls on acoustic communication, noting that the pipe is not in direct contact with concrete walls in some buildings and industries. If this condition is not met, a concrete wall can represent a significant signal-damping factor, making acoustic communication infeasible. In such cases, the signal must pass through the walls via electric signals traveling in wires after conversion. Additionally, acoustic signal reflections can degrade the signal quality since they can cause interference with the direct waves. In this paper, reflections are present but are neglected in the initial stages of the research.

Maritime transportation is another field where acoustic communication is favored [12]. In this application, wired communication is affected by many problems, especially cable susceptibility and limited capacity.

Huang et al. [13] discusses the transmission of acoustic waves through solids. Specifically, wave transmission was implemented using an ElectroMagnetic Acoustic Transducer (EMAT) transmitter in the ultrasonic frequency range (f > 20 kHz). In addition to data transmission, a Wireless Power Transfer (WPT) through metallic structures has also been implemented. In this regard, [14] presents the possibility of achieving power transmission using acoustic mechanical vibrations, with a power transfer efficiency of 33%. Another example of Wireless Power Transfer is dealt with in [15], where the transmission of power is discussed together with the communication on metallic structures. The advantage of this approach is the collection of energy even in places lacking electrical power sources. In [16], in addition to a WPT in metallic structures via acoustic waves, optimizing was also assessed by varying the transmission angle with respect to the channel. To achieve this, a simulation of acoustic wave propagation in various cases is presented. This paper will consider only data transmission by mechanical acoustic waves in metallic structures.

Schaechtle et al. [17] present an implementation of data transmission using passive mechanical sensors, exploiting their natural resonance frequency and communicating in the ultrasonic frequency band. It also presents the results of acoustic communication at lower frequencies.

Data transmission over metallic structures using acoustic waves is described in [18], which particularly deals with the software to drive the output signal with an ARM-based Application-Specific Integrated Circuit (ASIC) processor. A discussion about acoustic communication using On–Off Keying (OOK) modulation is also reported in [19], where data transmission is established on metallic pipelines. This work describes data transmission through Chirp-OOK modulation and demodulation on an ASIC architecture, while the authors aim to realize communication using a Field-Programmable Gate Array (FPGA).

2.1. Article Contributions and Novelty

An important contribution is the hardware design of the acoustic transmitter and receiver via FPGA, using a RISC-V architecture [20], which makes the implementation, unlike the ASIC version, more versatile and adaptable to the user's needs. It also allows

the creation of modules via a Verilog description of the hardware. An additional novelty is the creation of a conditioning circuit printed on a board, considering the boundary conditions. The Printed Circuit Board (PCB), placed between the FPGA and the acoustic actuator/transducer, has been developed to communicate efficiently on a metal bar using acoustic waves on the transmit and receive sides. It includes filters and amplifiers to optimize signal transmission. The description of the transmitted and received signal, the reasoning, and the mathematical considerations behind the design of the modulation and demodulation circuits and the conditioning PCB are described in Section 3. The advantage of the approach proposed in this application is to avoid wired or wireless communication in an environment generally characterized by metallic structures, a critical factor for electromagnetic interference.

3. Experimental Tests and Results

Before implementing acoustic communication, the boundary conditions must be defined to design the communication circuit properly. To this end, the three aspects of the proposed approach, presented in Section 3.1, are analyzed. Their discussion is provided in three different experiments in this section.

3.1. Study of the Acoustic Noise Response of a Metal Structure

Although acoustic communication can avoid problems related to electromagnetism, acoustic noise is also present in the industrial environment. This subsection aims to simulate and measure acoustic noise levels and construct a noise profile along a metallic bar by varying its length.

As a first step, a frequency analysis was simulated with the software SolidWorks to evaluate the expected frequency response of the metallic bar and, thereby, understand the most suitable frequency value for the carrier wave. The simulations were performed on three aluminum bars as metallic structures, which were 70 cm-, 140 cm-, and 280 cm-long, respectively. The bar was excited from one edge with a force magnitude of 1 N, and the acceleration at the other edge was evaluated at different frequencies. The results of the simulations are reported in Figure 1, which shows that, for the 70 cm-long bar, there is a high-pass response with a peak at almost 2 kHz that becomes almost flat for frequency values higher than 4 kHz. Regarding the simulation of the 140 cm- and 280 cm-long bars, the frequency response is also characterized by a low-pass response. On the y-axis in Figure 1, the curves report the mean frequency behavior of the accelerations relative to the maximum acceleration value. The simulations present the behavior of the system with several bar length values. The simulations are based on the theory of propagation of elastic waves, supported by Lagrange's equations of motion, Euler–Bernoulli's beam theory, and Rayleigh and Timoshenko's beam theory, which leads to partial differential equations [21,22], which are not solvable in a closed form but only through numerical solutions given by a finite element method. After the simulations, a complete frequency characterization of the whole system (acoustic transducers + 70 cm aluminum bar) was performed in a real scenario to choose the optimal carrier frequency for communication and the noise profile construction. A 70 cm-long aluminum bar has been used to arrange an experimental setup. Two SCM-401R acoustic piezoelectric devices have been placed on the metal bar. The SCM-401R can be used as a sensor and actuator of acoustic waves. The frequency analysis was performed with a fixed distance, placing the actuator and the transducers at the opposite edges of the hanging bar. In this experiment, one device is connected to a waveform generator [23], which applies the acoustic waves on the metal bar and functions as an actuator. The other, connected to an oscilloscope, acts as a transducer, converting the acoustic signal into a voltage level.

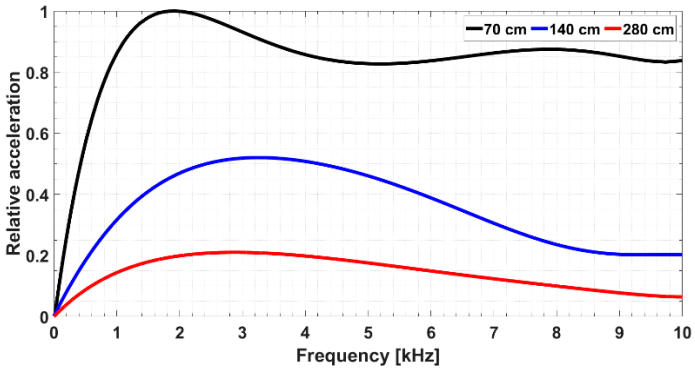

Figure 1. Simulation results of the frequency response for the 70 cm- (black curve), 140 cm- (blue curve), and 280 cm-long (red curve) aluminum bars.

In this way, the intensity of acoustic waves at the receiver side can be measured. To perform this test, the bar has been hung at the ends using a nylon thread so as not to affect sound propagation. In addition, a thin layer (<1 mm) of beeswax has been interposed between each acoustic device and the bar under test to ensure electrical isolation between the piezoelectric devices and the metallic bar. Furthermore, as demonstrated in its datasheet [24], the piezoelectric device is characterized by a maximum directional radiation pattern in the direction orthogonal to the frontal surface of the device itself. This maximizes the acoustic impedance matching, making the acoustic wave fraction that propagates in the air as negligible as possible with respect to the fraction that propagates in the metal rod.

The results of the frequency analysis are shown in the graph in Figure 2 (blue curve). The frequency response in the real scenario aligns with the simulation in Figure 1 results, showing a flat frequency response in the second part of the characteristic. The difference in the real case with respect to the simulation is the higher cutoff frequency, which results in around 5 kHz. The frequency response of the transducer causes this effect. In fact, the received signal is low in the 1–5 kHz range because the piezoelectric device is too small to support vibrations in such a range of frequencies. By considering the results of the previous experiments, the carrier frequency for the communication between the acoustic devices should be chosen to be as low as possible since, as presented in [25] and also shown in this paper in Figure 1, if the communication distance increases and the material is the same, the metallic structure behaves as a low-pass filter with respect to the elastic waves. Based on the results obtained, the carrier frequency for the OOK modulation has been chosen to be equal to 5 kHz for the following reasons:

- it is the lowest frequency in the band of the transducer;
- it is the farthest frequency from the transducer resonance, which, according to the datasheet, is 40 kHz.

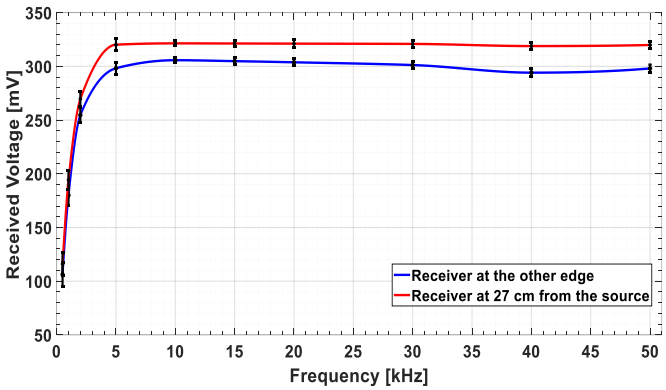

Figure 2. Frequency response of the communication system.

Although the transducer resonance frequency can be used as the carrier wave frequency in some cases, the resonance effect represents a disturbing factor in this case because, in the OOK modulation, even when the transmitted bit is a logical zero, the demodulated signal is superimposed with the resonance signal. Moreover, it is important to choose a carrier frequency far from the resonance because, in this way, the resonance can be easily removed using a first-order RC filter.

Evaluating the transducer frequency was also useful for setting up the study of the noise profile along the bar. The characterization of the noise profile on the bar was carried out with an injected sinusoidal noise of 5 kHz and 5 V amplitude. The experiment was conducted by implementing the measurement setup shown in Figure 3, moving the sensor in the direction opposite to the source along the bar and evaluating the received noise every 3 cm. To minimize the influence of high-frequency noise on the measured values, 30 measurements were taken at each point along the bar to calculate the mean and the standard deviation of the received voltage signal.

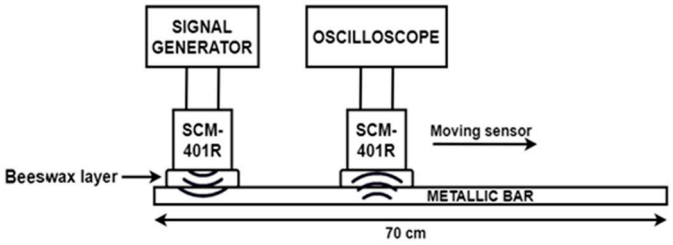

Figure 3. Schematic diagram of the noise measurement experiment.

Figure 4 presents the findings from the noise profile experiment. As depicted in the figure, the highest noise level is recorded at a position 27 cm from the source, which represents the most problematic location in terms of acoustic interference. Once this point was identified, a frequency analysis was carried out with the receiver at this position, and the results are shown in Figure 2 (red curve). As predicted, the frequency response in this scenario shifts slightly upwards. Although the noise profile was assessed, as demonstrated in Figure 4, by measuring the voltage at all 22 positions along the metallic bar, the two locations (27 cm and the end of the bar) are, under the current setup, the most relevant when evaluating acoustic communication and noise impact.

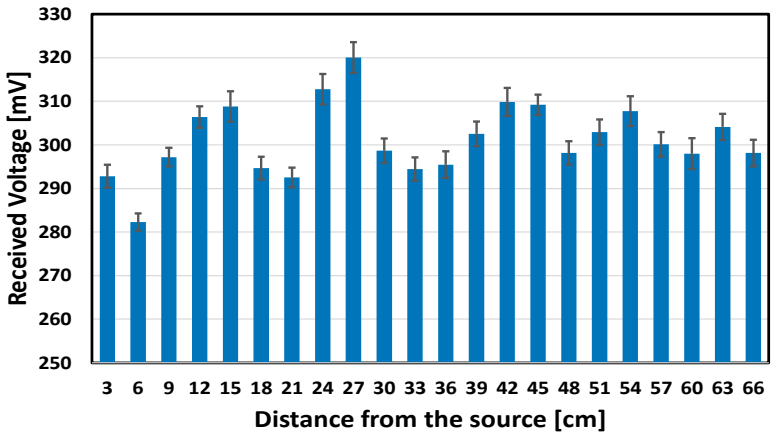

Figure 4. Results of the noise profile analysis.

This result is significant because it will be used to evaluate the impact of noise on acoustic communication in Section 4.

3.2. Communication Using Acoustic Waves

The communication attempt was also conducted using the "hanging bar" configuration, with the acoustic transducers positioned at the ends of the bar. This time, sinusoidal signals modulated with OOK were transmitted. There are several reasons for choosing OOK modulation. Firstly, this modulation is straightforward and is commonly used in short-range wireless applications, such as home automation, remote keyless entry, and wireless base stations. One noteworthy application of this modulation pertains to industrial networks, which is the focus of this paper. Unlike other protocols (such as FSK and ASK), OOK modulation is notably energy-efficient because it does not transmit a signal when sending a bit "0". This characteristic results in lower power consumption, which is demonstrated in [26], through a battery discharge study.

On the other hand, more complex modulations generally require more power, which can be a significant disadvantage in energy-sensitive applications. For instance, in [27] an experiment of signal transmission on the pipeline surface illustrates this issue. In such an environment, energy saving is crucial to ensure a long-life node; thus, a low-power communication protocol is required.

Additionally, energy-harvesting solutions can be incorporated alongside a Power Management System (PMS) and powered with several techniques, such as solar cells [28], Microbial Fuel Cells [29], or small wind turbines [30]. For these reasons, and due to its relative simplicity compared to other techniques, OOK modulation is the preferred choice for this initial stage of research. The signal processing has been implemented on an FPGA using the RISC-V architecture. An FPGA was selected due to its greater flexibility compared to ASIC circuits and the ability to add modules, such as a custom-designed OOK modulation and demodulation module. Additionally, an FPGA architecture provides a set of registers that can be easily accessed externally via software once the hardware is described on the FPGA.

For the transmission, an Artix7 FPGA mounted on a Digilent NexysA7 Board is used. Since it only includes digital pins, the signal must be modulated using Pulse Width Modulation (PWM), requiring a Digital-to-Analog Converter (DAC) in the modulation circuit. The formula defining the PWM operation is shown in Equation (2).

$$V_{out} = DV_{in} \tag{2}$$

where V_{in} represents the high logic level of the FPGA (3.3 V), V_{out} is the output voltage, and D is the duty cycle of the digital square wave. To create a square wave with a variable duty cycle on the FPGA, a counter increments with each positive edge of the internal clock. The counter is initially set to 0, and the output signal starts at a high logic level. When the counter reaches a specified value, the output signal switches to low for the remainder of the square wave period; at the end of the period, the counter resets to 0, and the cycle restarts. This process generates a square wave with a variable duty cycle. To produce a sinusoidal signal at the output, the duty cycle D must vary in a sinusoidal pattern. This condition is expressed in Equation (3).

$$V_{out}(t) = D(t)V_{in} = V_{in}\sin(2\pi ft), \tag{3}$$

where f is the frequency of the output sinusoidal signal. For a given clock frequency—50 MHz for the RISC-V architecture—the total count N required to produce a sinusoidal signal at the desired frequency is given by Equation (4).

$$N = \sqrt{\frac{f_{clock}}{f_{out}}} \tag{4}$$

The f_{clock} limit in the FPGA does not allow it to reach a too-high output signal frequency. A schematic explanation of the sine wave generation is shown in Figure 5.

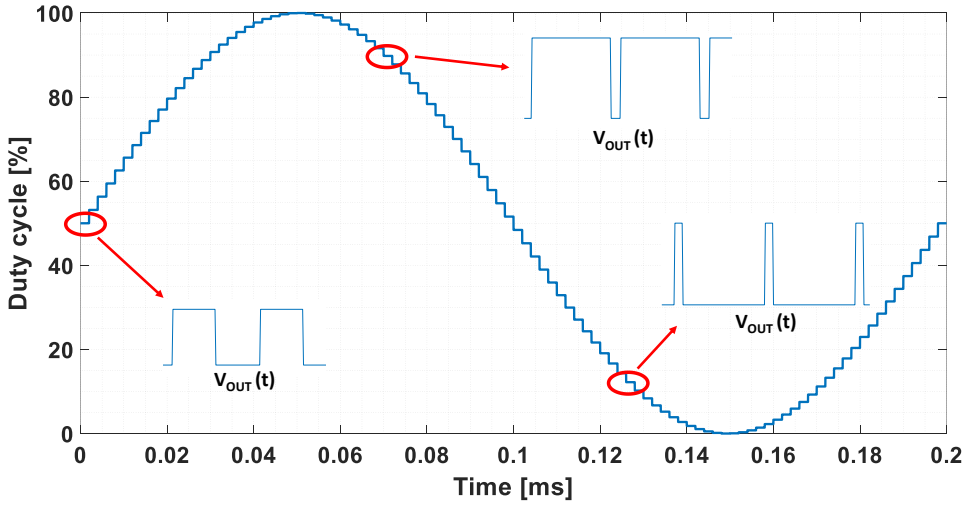

Figure 5. Trend over time of the Vout duty cycle "D".

As shown in the figure, the sinusoidally varying duty cycle implies a V_{OUT} with a variable duty cycle, which is the waveform that comes out from the FPGA board. This results in a clean sinusoidal wave after the RC filter.

According to Equation (4), the higher the frequency of the generated carrier wave, the lower its output quality is. In fact, as f_{out} increases, for the same f_{clock} value, the number N of points per period decreases, resulting in an output signal with a worse quality with respect to an output signal with a lower frequency.

If this consideration is added to the factors listed in Section 3.1, the chosen carrier frequency is set to 5 kHz. To produce a 5 kHz sinusoidal signal, the counter must reset to 0 after a total of 100 counts. Meanwhile, the predetermined value where the output signal switches to 0 is determined by the desired instantaneous amplitude of the sinusoidal output at that moment. This approach creates a 500 kHz square wave with 100 distinct duty cycle values. To achieve a clean sinusoidal signal free of any DC component, the resulting square wave is filtered through a band-pass circuit, which is built by cascading a low-pass filter and a high-pass filter, positioned on the "modulator side" of the PCB, as shown in Figure 6a. To further minimize the effects of the 500 kHz PWM, the low-pass filter's cutoff frequency should be placed just above the 5 kHz carrier frequency.

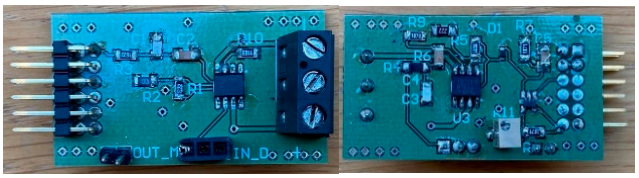

(**a**) (**b**)

Figure 6. Custom-made PCB with two layers: (**a**) modulation layer; (**b**) demodulation layer.

OOK modulation is used to encode the analog signal as a bitstring. To transmit a "1", eight cycles of the sinusoidal signal are sent to the output. To transmit a logical "0", a constant voltage is applied by setting the PWM duty cycle to 50% for the entire bit duration. With these settings, the bit duration is 1600 µs. The conditioning circuit includes a band-pass filter and an amplifier to remove the DC component and suppress the actuator's resonance frequency (40 kHz), as well as an amplifier to boost the signal before transmitting it along the metal bar via the acoustic actuator.

After presenting the modulation process, it is necessary to explain the demodulation process that occurs after the signal travels along the metal bar. The received signal is amplified through an operational amplifier in a non-inverting configuration. Oscilloscope

measurements show that the output of the receiving amplifier reaches an amplitude of 6 V. To demodulate the received signal, an OOK demodulation circuit is used, consisting of a quasi-peak detector circuit followed by a comparator with an adjustable threshold. Both circuits are located on the bottom layer of the PCB. The "demodulation layer" of the PCB is shown in Figure 6b. The peak detector and comparator must be configured so that when a "1" is transmitted the output of the peak detector remains consistently above the comparator's threshold. Conversely, when a "0" is transmitted the peak detector output must stay fully below the comparator threshold. The advantage of this approach is that it enables efficient demodulation of the signal and ensures accurate reception of the transmitted bitstring. However, this method has some drawbacks. Firstly, there are delays in the switching of the demodulated signal relative to the carrier wave caused by the comparator's threshold level. The delay in transitioning from 0 to 1 is given by Equation (5).

$$\Delta t_{0\to 1} = \frac{1}{2\pi f}\sin^{-1}\left(\frac{V_{TH}}{V_{PK}}\right) \tag{5}$$

where V_{TH} is the voltage threshold for the comparator, which triggers the output to switch from 0 to 1 when this level is exceeded, V_{PK} represents the peak amplitude of the received sine wave (6 V), and f is its frequency. Equation (5) holds as long as f is within the frequency range that the peak detector can handle while the capacitor is charging. This range is quite broad because the capacitor charges through a low-resistance path when the diode is active (ON). Therefore, the assumption $f < 1/(20\pi \times R_{diode} \times C)$ is easily satisfied. This is why $\Delta t_{0\to 1}$ can be expressed only in terms of the signal's characteristics and the comparator threshold, making the effects of the diode's resistance and the capacitor's value negligible. The delay for switching from 1 back to 0 is given by Equation (6).

$$\Delta t_{1\to 0} = RC\ln\left(\frac{V_{PK}}{V_{TH}}\right) - \frac{3}{4f}\,, \tag{6}$$

where R and C are the peak detector's resistance and capacitance values, respectively. These components have been dimensioned with 36 kΩ and 6 nF, respectively. These components have been configured with 36 kΩ and 6 nF, respectively. These values were chosen empirically to achieve a balanced compromise between the two delays. As can be observed, the two delays exhibit opposite characteristics:

- $\Delta t_{0\to 1}$ increases as the signal frequency decreases and becomes smaller when the comparator threshold is smaller.
- $\Delta t_{1\to 0}$ increases as the comparator threshold decreases and becomes smaller when the signal frequency is smaller.

In addition, to avoid commutations at the wrong times, V_{TH} must be included in the interval $0 < V_{TH} < V_{PK}e^{-\frac{t^*}{RC}}$, where t* is the first non-zero solution of Equation (7).

$$V_{PK}\, e^{-\frac{t^*}{RC}} = V_{PK}\cos(2\pi f t^*) \tag{7}$$

If this condition is not met, multiple crossings occur at the comparator threshold during the high logic level of the peak detector output, leading to incorrect switching when transmitting a "1" bit. A voltage divider was used to make V_{TH} adjustable by dividing the 3.3 V from the FPGA pin.

Considering the switching delays in Equations (5) and (6), the worst-case scenario, where most switching events occur, is the bit sequence 10101010, corresponding to 0xAA. Along with the message, on the transmission side, the FPGA is programmed to generate a start bit and a stop bit around the transmitted byte. Once the required hardware is described on the FPGA, the message can be created by interfacing the FPGA with the PlatformIO software and programming it in C.

Conditioning circuits were implemented to modulate and demodulate the signals, allowing the FPGA to interface with the acoustic actuator. The practical setup for the entire

communication system is shown in Figure 7. As illustrated, communication takes place through the implemented PCBs, which transmit the signal to the acoustic actuator. The actuator on the other end of the bar receives the signal and sends it to the FPGA. As shown in Figure 7, the oscilloscope displays the signal along the metal bar (depicted as the yellow track) and, after demodulation, the output of the peak detector (cyan track). The FPGA processes the bitstring and converts it into a 1-byte hexadecimal message on the receiving end. This decoding is managed by a Finite State Machine (FSM), implemented on the FPGA, which is triggered by the rising edge of the start bit from the comparator. This ensures that the FPGA is synchronized with the incoming bit stream. To sample the next bit correctly, the FSM waits for 1.5 bit times (2400 µs), aligning it with the center of the bit. After the first bit, it samples every subsequent bit at the center (1600 µs per bit). Once eight bits are received, the entire byte is stored as the decoded message. In conclusion, it has been shown that OOK modulation for data transmission via acoustic waves over metallic structures is a viable method. With the actual conditions, the bit rate in communication results to be 6.25 kbit/s.

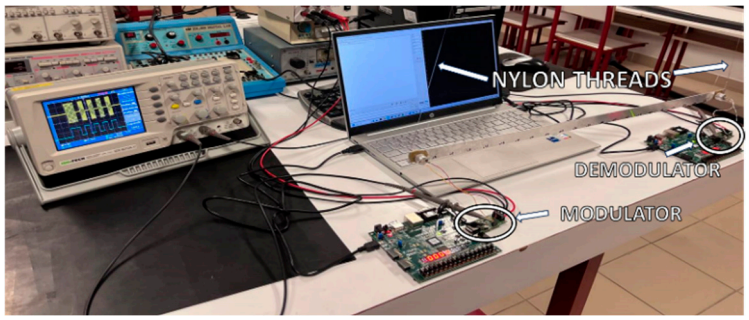

Figure 7. Experimental setup for acoustic communication.

4. Evaluation of the Noise Influence on the Sent Bitstrings

This subsection builds upon the findings from Sections 3.1 and 3.2 to assess the performance of the acoustic communication system described in Section 3.2 within a noisy environment. As illustrated in Figure 8, in addition to the experimental setup detailed in Section 3.2, a noise factor is introduced in this case. The noise generator in Figure 8 is configured to emit sinusoidal noise at various frequencies, with a maximum amplitude of 6 V, which matches the amplitude of the received signal after amplification, as explained in Section 3.2. The noise source is positioned 27 cm from the transmitter, as this distance represents the worst-case scenario for communication interference, as shown in Section 3.1.

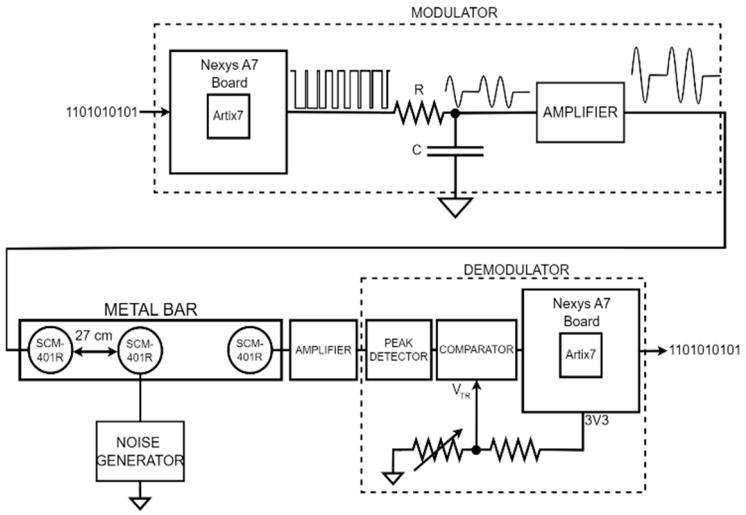

Figure 8. Experimental setup for acoustic communication.

Under these conditions, packet loss *(PL)*, defined by Equation (8), is used as the key metric to evaluate the quality of the communication.

$$PL_{\%} = \left(1 - \frac{bytes\ correctly\ received}{total\ bytes}\right) \times 100 \tag{8}$$

The message transmitted consisted of 1 byte, corresponding to the hexadecimal value 0xAA. To achieve this, a sequence of 1000 packets was sent, and the packet loss was evaluated based on the frequency and amplitude of the noise. The packets were transmitted and received using MATLAB's "serial plot" command. By knowing the number of transmitted packets, a comparison between the sent and received data was made, and the packet loss was calculated using Equation (8).

The results of this test are shown in Figure 9, where the frequency responses of PLs at different noise amplitudes are normalized with respect to the 6 V maximum value of 6 V injected noise and expressed in dB.

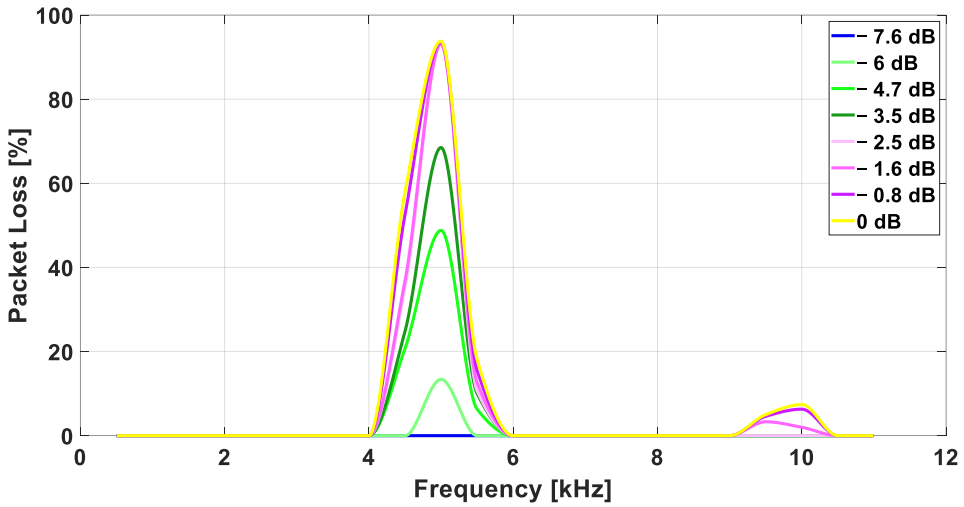

Figure 9. Frequency vs. packet loss at various noise amplitude levels.

As can be seen, the response matches the expected behavior. In fact, it exhibits a peak around the frequency of 5 kHz, which is the frequency of the modulated carrier wave used for acoustic communication. In addition, the PL increases for higher noise amplitudes (purple and yellow curves). In contrast, at lower noise levels (blue curve), the noise becomes significantly disturbing for injected noise amplitudes above -6 dB (3 V). As can also be seen, there is a small value of PL around the frequency of 10 kHz, which is a multiple of the carrier wave of 5 kHz. This effect is due to the non-ideality of the sinusoidal noise applied to the bar. In general, the PL contribution after 10 kHz is greatly attenuated due to the low-pass filter inserted in the modulation circuit to reduce the PWM effect and in the demodulator after the aluminum bar to decrease the resonance effect of the acoustic transducer. It can be concluded that the noise rejection test showed promising results, as communication becomes inefficient only at higher frequencies compared with the usual industrial applications since, in most cases, acoustic noise does not occur at frequencies higher than a few hundred hertz. An evaluation process and frequency analysis of acoustic noise in the industry field are reported in [31].

This makes communication through acoustic waves an interesting research topic that will be further studied and improved in future work.

5. Discussion and Conclusions

Based on the contents presented, the following considerations can be drawn. Implementing wireless communication among metallic structures is almost impossible due

to their high conductivity and, consequently, high reflection coefficient. This can cause multipath and interference between direct and multiple reflected electromagnetic waves. Therefore, an alternative way to establish communication in these environments is needed. This work demonstrated the feasibility of communicating through acoustic waves from piezoelectric materials and applying mechanical waves on metal structures. Based on the literature, the initial analog front-end was implemented, and, as a novel approach, the physical characteristics of a metal bar under acoustic wave excitation were studied to construct a noise profile response along the length of the bar. This study was important in defining the boundary conditions of communication and digital modulations, which was the next experiment (carrier frequency, distance from the source, and so on). The study of physical characteristics was also crucial to assess the communication packet loss. In fact, in this experiment, it was seen that at a frequency of about 5 kHz, the carrier frequency of the data sent, the communication is characterized by the highest number of erroneous messages received, and thus the highest percentage of packet loss (93.8%).

Future developments in this field will involve WPT with FPGA by applying acoustic waves and trying to communicate at higher frequencies by choosing another acoustic device with a different resonance frequency. A higher carrier frequency implies a shorter bit time and a higher transmission speed. Better communication performances can also be reached by implementing another more complicated but better-performing modulation than the OOK one. Other improvements may concern the demodulation circuit. In particular, an adjustable-gain amplifier with variable resistors has been implemented to adapt the received amplified level to a chosen fixed level, regardless of the distance from the signal source. In addition, the comparator can be implemented in a non-inverting Schmitt trigger configuration, which introduces a hysteresis band, allowing for a reduction in the delays present in the peak detector circuit. Finally, communication standardization can be implemented: for example, by using the IEEE 1451 protocol to build smart networks capable of exchanging data on metallic structures using acoustic waves. With this aim, future work involves implementing a network of sensors and their communication, assigning an address to each sensor, and using metal structures as the propagation medium and modulated acoustic signals to transmit data.

Author Contributions: Conceptualization, A.E.-S., V.P. and J.S.; Methodology, P.C., V.P. and J.S.; Software, P.C. and J.S.; Validation, A.E.-S. and J.S.; Investigation, A.E.-S. and V.P.; Resources, A.E.-S. and V.P.; Writing—original draft, P.C., H.d.R. and J.S.; Writing—review & editing, H.d.R.; Supervision, A.E.-S., V.P. and J.S. All authors have read and agreed to the published version of the manuscript.

Funding: Helbert da Rocha and António Espirito-Santo were financially supported by the Project GreenAuto: Green Innovation for the Automotive Industry, NO. C644867037-00000013, investment project nr. 54, from the Incentive System to Mobilizing Agendas for Business Innovation, funded by the Recovery and Resilience Plan and by European Funds NextGenerationEU.

Data Availability Statement: No new data were created or analyzed in this study. Data sharing is not applicable.

Conflicts of Interest: The authors declare no conflict of interest.

References

1. Rout, A.; Deepak, B.B.V.L.; Biswal, B.B. Advances in Weld Seam Tracking Techniques for Robotic Welding: A Review. *Robot. Comput. Integr. Manuf.* **2019**, *56*, 12–37. [CrossRef]
2. Phuyal, S.; Bista, D.; Bista, R. Challenges, Opportunities and Future Directions of Smart Manufacturing: A State of Art Review. *Sustain. Futures* **2020**, *2*, 100023. [CrossRef]
3. Zhang, Z.; Chen, S. Real-Time Seam Penetration Identification in Arc Welding Based on Fusion of Sound, Voltage and Spectrum Signals. *J. Intell. Manuf.* **2017**, *28*, 207–218. [CrossRef]
4. Taylor, C.D.; Gutierrez, S.J.; Langdon, S.L.; Murphy, K.L.; Walton, W.A. Measurement of RF Propagation into Concrete Structures over the Frequency Range 100 MHz to 3 GHz. In *Wireless Personal Communications*; Springer US: Boston, MA, USA, 1997; pp. 131–144.
5. Caruso, P.; Iacono, S.D.; Di Caro, D.; Paciello, V. Pipeline Characterization for Communication Channel Properties Improvement. *IEEE Trans. Instrum. Meas.* **2024**, *73*, 1–10. [CrossRef]

6. Mapunda, G.A.; Ramogomana, R.; Marata, L.; Basutli, B.; Khan, A.S.; Chuma, J.M. Indoor Visible Light Communication: A Tutorial and Survey. *Wirel. Commun. Mob. Comput.* **2020**, *2020*, 1–46. [CrossRef]
7. Chen, M.; Ma, Z.; Chen, X.; Owais, M.; Liu, Y. A Calibration Strategy for Smart Welding. In Proceeding of International Conference on Image and Graphics, Haikou, China, 6–8 August 2021; pp. 3–17.
8. Saniie, J.; Wang, B.; Huang, X. Information Transmission Through Solids Using Ultrasound Invited Paper. In Proceedings of the 2018 IEEE International Ultrasonics Symposium (IUS), Kobe, Japan, 22–25 October 2018; IEEE: Washington, DC, USA, 2018; pp. 1–10.
9. Hosman, T.; Yeary, M.; Antonio, J.K. Design and Characterization of an MFSK-Based Transmitter/Receiver for Ultrasonic Communication Through Metallic Structures. *IEEE Trans. Instrum. Meas.* **2011**, *60*, 3767–3774. [CrossRef]
10. Heifetz, A.; Saniie, J.; Huang, X.; Wang, B.; Shribak, D.; Koehl, E.R.; Bakhtiari, S.; Vilim, R.B. *Final Report for Transmission of Information by Acoustic Communication along Metal Pathways in Nuclear Facilities*; Argonne National Lab: Argonne, IL, USA, 2019. Available online: https://publications.anl.gov/anlpubs/2019/11/157041.pdf (accessed on 29 October 2023).
11. Heifetz, A.; Bakhtiari, S.; Huang, X.; Ponciroli, R.; Vilim, R.B. *First Annual Progress Report on Transmission of Information by Acoustic Communication Along Metal Pathways in Nuclear Facilities*; Argonne National Lab: Argonne, IL, USA, 2017.
12. Lee, J.; Bae, J.; Lee, C.H. Waseem Abbas Ultrasonic Sensor Communication System Using Steel Structures in Ship. In Proceedings of the 7th international conference on Advanced Materials, Development and Performance, Singapore, 29 July–1 August 2014.
13. Huang, X.; Saniie, J.; Bakhtiari, S.; Heifetz, A. Ultrasonic Communication System Design Using Electromagnetic Acoustic Transducer. In Proceedings of the 2018 IEEE International Ultrasonics Symposium (IUS), Kobe, Japan, 22–25 October 2018; IEEE: Washington, DC, USA, 2018; pp. 1–4.
14. Tseng, V.F.-G.; Bedair, S.S.; Lazarus, N. Acoustic Power Transfer and Communication With a Wireless Sensor Embedded Within Metal. *IEEE Sens. J.* **2018**, *18*, 5550–5558. [CrossRef]
15. Oppermann, P.; Renner, B.-C. Acoustic Backscatter Communication and Power Transfer for Batteryless Wireless Sensors. *Sensors* **2023**, *23*, 3617. [CrossRef] [PubMed]
16. Litman, R.B.; Wilt, K.R.; Scarton, H.A.; Saulnier, G.J. Shear and Longitudinal Acoustic Communication and Power Transfer Through Plates Using Acoustic Wedges. In Proceedings of the Volume 13: Vibration, Acoustics and Wave Propagation, American Society of Mechanical Engineers, Montreal, QC, Canada, 14–20 November 2014; p. V013T16A032.
17. Schaechtle, T.; Kar, B.; Fischer, G.K.J.; Gabbrielli, A.; Hofiinger, F.; Wallrabe, U.; Rupitsch, S.J. Acoustically Coupled Passive Wireless Sensor System With Mechanical Resonant Sensor. In Proceedings of the 2022 IEEE International Conference on Wireless for Space and Extreme Environments (WiSEE), Winnipeg, MB, Canada, 12–14 October 2022; IEEE: Washington, DC, USA, 2022; pp. 39–43.
18. Caruso, P.; Iacono, S.D.; Paciello, V. Data Transmission Using FSK Modulation on an Unconventional Channel. In Proceedings of the 2023 IEEE International Workshop on Metrology for Industry 4.0 & IoT (MetroInd4.0&IoT), Brescia, Italy, 6–8 June 2023; IEEE: Washington, DC, USA, 2023; pp. 36–41.
19. Wang, B.; Saniie, J.; Bakhtiari, S.; Heifetz, A. Software Defined Ultrasonic System for Communication Through Solid Structures. In Proceedings of the 2018 IEEE International Conference on Electro/Information Technology (EIT), Rochester, MI, USA, 3–5 May 2018; IEEE: Washington, DC, USA, 2018; pp. 267–270.
20. Harris, S.L.; Chaver, D.; Pinuel, L.; Gomez-Perez, J.I.; Liaqat, M.H.; Kakakhel, Z.L.; Kindgren, O.; Owen, R. RVfpga: Using a RISC-V Core Targeted to an FPGA in Computer Architecture Education. In Proceedings of the 2021 31st International Conference on Field-Programmable Logic and Applications (FPL), Dresden, Germany, 30 August 2021–3 September 2021; IEEE: Washington, DC, USA, 2021; pp. 145–150.
21. Piersol, A.G.; Paez, T.L.; Harris, C.M. *Harris' Shock and Vibration Handbook*, 6th ed.; McGraw-Hill: New York, NY, USA, 2010.
22. Hambric, S.A. Structural Acoustics Tutorial—Part 1: Vibrations in Structures. *Acoust. Today* **2006**, *2*, 21. [CrossRef]
23. TG210 2MHz Function Generator from TTi, Datasheet. Available online: https://www.google.com/url?sa=t&source=web&rct=j&opi=89978449&url=https://docs.rs-online.com/6947/0900766b80d05751.pdf&ved=2ahUKEwi6yIqkz--JAxWQdPUHHblUAJMQFnoECB0QAQ&usg=AOvVaw1txxMQjBPVtyBi52qQ7Z_4 (accessed on 29 October 2023).
24. SCM-401R Acoustic Piezoelectric Sensor/Transducer, Datasheet. Available online: https://www.google.com/url?sa=t&source=web&rct=j&opi=89978449&url=https://www.ret.hu/media/product/15343/438381/SCS-SCM_401.pdf&ved=2ahUKEwiapZPPz--JAxXcia8BHeuOE5AQFnoECBgQAQ&usg=AOvVaw133ZZsWkcdEhJ9MJeB7eaK (accessed on 29 October 2023).
25. Kiziroglou, M.E.; Boyle, D.E.; Wright, S.W.; Yeatman, E.M. Acoustic Power Delivery to Pipeline Monitoring Wireless Sensors. *Ultrasonics* **2017**, *77*, 54–60. [CrossRef] [PubMed]
26. Shen, T.; Wang, T.; Sun, Y.; Wu, Y.; Jin, Y. On the Energy Efficiency of On-Off Keying Transmitters with Two Distinct Types of Batteries. *Sensors* **2018**, *18*, 1291. [CrossRef] [PubMed]
27. Caruso, P.; Iacono, S.D.; Paciello, V. Exploiting Gas Pipelines as an Unconventional Communication Channel. In Proceedings of the 2023 IEEE International Conference on Computational Intelligence and Virtual Environments for Measurement Systems and Applications (CIVEMSA), Gammarth, Tunisia, 12 June 2023; IEEE: Washington, DC, USA, 2023; pp. 1–6.
28. Ullah, S.; Hafeez, G.; Rukh, G.; Albogamy, F.R.; Murawwat, S.; Ali, F.; Khan, F.A.; Khan, S.; Rehman, K. A Smart Sensors-Based Solar-Powered System to Monitor and Control Tube Well for Agriculture Applications. *Processes* **2022**, *10*, 1654. [CrossRef]
29. da Rocha, H.; Caruso, P.; Pereira, J.; Serra, P.; Espirito Santo, A. Discussion on Secure Standard Network of Sensors Powered by Microbial Fuel Cells. *Sensors* **2023**, *23*, 8227. [CrossRef] [PubMed]

30. Wang, H.; Xiong, B.; Zhang, Z.; Zhang, H.; Azam, A. Small Wind Turbines and Their Potential for Internet of Things Applications. *iScience* **2023**, *26*, 107674. [CrossRef] [PubMed]
31. Caruso, P.; da Rocha, H.; Paciello, V.; Salvado, J.; Espírito-Santo, A. Advanced Smart Sensing Node with Acoustic-Based Connectivity for Spot Welding in the Automotive Industry. In Proceedings of the 2024 IEEE International Instrumentation and Measurement Technology Conference (I2MTC), Glasgow, UK, 20–23 May 2024; IEEE: Washington, DC, USA, 2024; pp. 1–6.